44th AIAA Aerospace Meeting and Exhibit, Reno, Nevada, 9-12 January 2006

The Turbulence Structure of Shockwave and Boundary Layer Interaction in a Compression Corner

M. Pino Martin*†, Alexander Smits‡, Minwei Wu* and Matthew Ringuette
Mechanical and Aerospace Engineering, Princeton University, Princeton, NJ 08540

Shockwave and turbulent boundary layer interactions (STBLI) result in intense localized heating rates and pressure loads, making them extremely important flow features that must be identified for engineering design. The absence of detailed and complete experimental and numerical data at the same flow and boundary conditions is one of the major stumbling blocks in the development of accurate turbulence models for the prediction of STBLI. We use a set of direct numerical simulation data (Wu & Martin, 2006) that has been validated against experiments (Bookey et al., 2005) at the same conditions to present detailed flow features of the STBLI over a compression corner at Mach 3 and low Reynolds number with Re_θ=2100. Details regarding the evolution of the turbulence structure angle, characteristic streamwise length scales, and hairpin packets through the interaction are presented. The three-dimensionality of the turbulence field and main shock are illustrated and the strength of shocks and shocklets through the interaction are considered.

Introduction

In supersonic and hypersonic flows, the interaction of shockwaves with turbulence is a characteristic flow feature that presents challenging problems in engineering design. These problems rapidly become more difficult as the Mach number increases, and in the hypersonic regime shockwave/turbulence interactions produce intense localized heating rates that can potentially compromise the integrity of the vehicle surface or engine. In addition, shock unsteadiness can lead to rapidly varying, intense pressure loads that can result in fatigue and structural failure. Thus, predicting and controlling the aerothermal loads caused by shockwave interactions in the turbulent flow regime is crucial to the efficient design of scramjet engines and hypersonic flight technology.

Many aspects of shock/turbulent boundary layer interactions (STBLI) are not fully understood, including the dynamics of shock unsteadiness, turbulence amplification, mean flow modification induced by shock distortion, separation and reattachment criteria, as well as the unsteady heat transfer near separation and reattachment points; and the generation of turbulent mixing layers and underexpanded jets in the interaction region, especially when they impinge on a surface. Most importantly, we need to predict and control the skin friction, pressure loads, and heat transfer accurately, given that the usual Reynolds analogies can lead to highly inaccurate results (see, for example, Evans & Smits, 1996). If we cannot predict the flow conditions we cannot expect to control them. Accurate predictions and scaling laws, and effective means for controlling the interaction regions can only be achieved by understanding the fundamental physics governing the dynamics of shockwave/turbulence interactions.

In 1998, the need to study shockwave/interaction via computations and experiments was recognized by NATO. That year, NATO established RTO Working Group 10 with a subgroup assigned to study shock-wave/turbulent-boundary layer interactions combining experiments and simulations. A great deal of insight is being gained from the efforts of this subgroup (Knight et al, 2002; Knight, 2002). However, the experiments and computations were not performed at the same Reynolds number, making the resulting disagreement among experimental and

* Member AIAA

‡ Fellow AIAA

computational data difficult to diagnose. A clear demonstration of this fundamental limitation was given in the DNS study of a compression ramp flow by Adams (2000) at Mach 3 and Re_θ 1685, where the comparable experimental data were only available at much higher Reynolds (~70,000), which prohibits drawing any definite conclusions, and prevents the development of general, robust turbulence models. For example, Rizetta and Visbal (2001) performed Large Eddy Simulations (LES) using a dynamic Smagorinsky model to calculate a similar flow. The results of the LES were compared against the DNS data of Adams (2000) and the available experimental data. However, the LES and DNS employed different inflow boundary conditions, and as already pointed out the experimental data were obtained at Reynolds number two orders of magnitude higher than the simulations. As a result, the agreement among the different data sets was only qualitative and the levels and sources of any disagreement were difficult to diagnose. It is also true that more engineering-type computations based on the Reynolds-averaged Navier-Stokes (RANS) equations (Zheltovodov, 2004; Sinha and Candler, 2005) show that state-of-the-art models do not give accurate predictions for all STBLI conditions. The absence of detailed and complete experimental and numerical data at the same inflow and boundary conditions is one of the major stumbling blocks to the development of accurate turbulence models for STBLI.

Ongoing research in the Princeton University Gas Dynamics and CROCCO Laboratories addresses the acknowledge lack of information and understanding that lies at the intersection of experimental and numerical research. In particular, we are performing experiments and simulations of the same flow configurations at the same Mach number, Reynolds number and boundary conditions, with the aim to validate the simulation data and to develop a greater understanding of STBLI, while establishing a database of traceable standardized STBLI flows that can be used to improve the fidelity of engineering turbulence models.

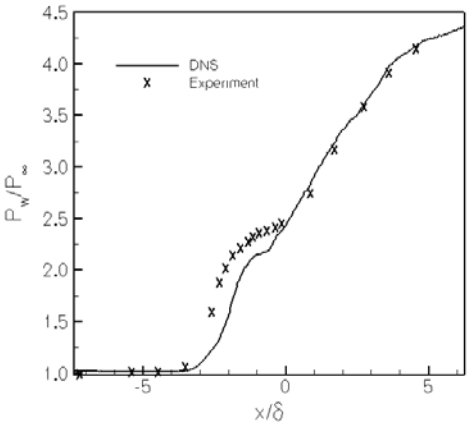

Figure 1: Surface-pressure distribution on a compression corner at Mach 3 and Re_θ=2400. The experimental and numerical data are from Bookey et al (2005) and Wu & Martin (2006), respectively.

The numerical/experimental collaboration has been challenging, but also extraordinarily fruitful. We have found remarkable agreement between the numerical and existing experimental data (in turbulence structure angles, velocity profiles, mass flux amplification, and skin friction coefficient), yet we have also found discrepancies in the wall pressure distribution due to limitations in the numerical methods. We would have not been able to find this subtle but important difficulty, nor its underlying cause, without detailed comparisons between experiment and simulation. Figure 1 plots the wall-pressure distribution for a STBLI over a compression corner at Mach 3 and Re_θ=2100 given from direct numerical simulation (DNS) and experiments. We have found that these flows are very sensitive to numerical dissipation. Whereas the data agree very well upstream and downstream of the corner, the size of the separation bubble in the DNS is 75% of that found in the experiment. Yet, this agreement is the best that has been achieved so far by any group concerned with this problem. Additional details on the numerical simulations and data can be found in Wu et al. (2005) and Wu & Martin (2006), on the numerical methods in Martin et al. (2005), Taylor et al. (2006) and on the experimental data in Bookey et al. (2005).

DNS provides a vast amount of accurate and detailed data that can be used to develop a greater understanding of fundamental physical phenomena and to develop and validate turbulence models that are true. In this paper, we present details about the STBLI in a compression corner configuration from the direct numerical simulation data of Wu & Martin (2006) at Mach 3 and Re_θ=2100. We first summarize the characteristics of the compression corner interaction case from existing experimental data. We then present additional details in the incoming boundary layer and through the interaction that can be observed from the DNS data. Of particular interest are the mean structure angle, integral length scale, three-dimensionality of the turbulent field, evolution of hairpin packets and the shock and shocklet strength through the interaction.

Background on the Compression Corner Interaction

The compression corner interaction is one of the simplest cases of STBLI that occur in internal and external vehicle flows. This configuration has been extensively studied experimentally by, for example, Settles et al. (1979), Kuntz et al. (1987), Smits & Muck (1987), Dolling and Murphy (1983), Ardonceau (1984), and Selig et al. (1989). The previous research covers a wide range of turning angles and Reynolds numbers, but the lowest Reynolds number reported from these studies is Re_θ = 23,000 (Settles et al., 1978). The upper Mach number is limited to about 5, corresponding to the experiments by Erengil & Dolling (1991). At higher Mach numbers, the interactions tend to be laminar (see, for example, Verma, 2003 for a compression corner study at Mach 9), and very little information is available on turbulent interactions at high Mach number, either experimentally or computationally. Recent experiments (Bookey et al., 2005) study the interaction at Mach 8.

The pressure gradient imposed by the shock can cause the flow to separate in the vicinity of the corner location, and at Mach 2.9 the flow is on the verge of separation with a corner angle of 16° (called incipient separation). At 24° and Re_θ=23,000, the time-averaged region of separation spans about 2δ starting approximately 1.2δ ahead of the corner and reattaching at about 0.8δ downstream of the corner. Near the line of separation, compression waves merge into a well-defined separation shock, and a second shock forms near the line of attachment (Settles, 1976). Figure 2 illustrates the flow over a compression corner configuration with increasing compression angle. The corresponding wall-pressure distribution shows an inflection point or "plateau" in the region of separation, as shown in Figure 3. Further downstream, the wall pressure eventually recovers to the inviscid oblique-shock value, but the point where this occurs is located farther downstream with increasing compression angle (Settles et al., 1978). For the 24° case, the inviscid value is not recovered at the end of the experimental model, nearly eight boundary layer thicknesses downstream of the corner.

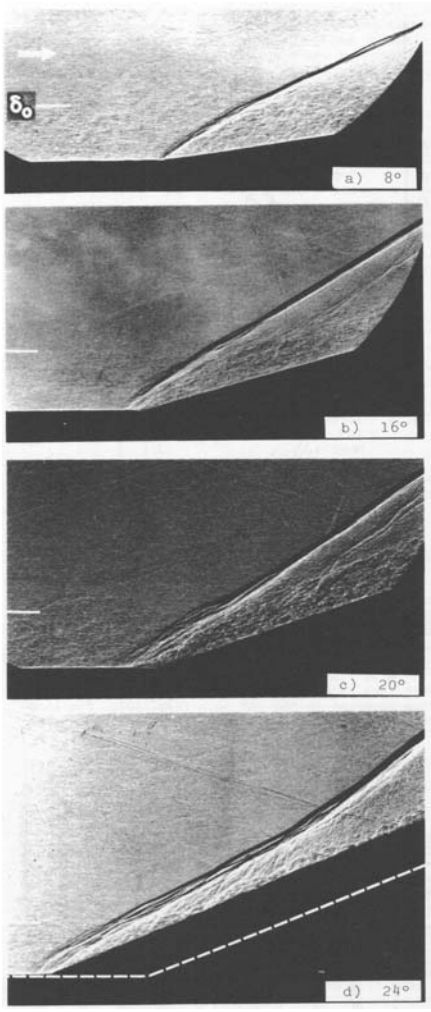

Figure 2: Shadowgraph images of Mach 2.85 compression corner interactions at various wedge angles (Settles et al, 1978)

A measure of the upstream influence is the distance from the corner at which the shock presence is first felt. A measure of the streamwise interaction extent is the separation length, being the distance between the separation and reattachment points. These characteristic lengths are determined from time-averaged measurements, and they vary with time due to the highly unsteady motion of the separation shock. The distance over which the separation shock moves increases with turning angle, and at 24° and Re_θ=23,000, it moves about 0.5δ (Selig et al., 1989). The frequency is typically an order of magnitude lower than any characteristic turbulence frequency, and of the order of 1 kHz. Thus, the frequency and scale of the shock motion are needed to fully characterize the interaction.

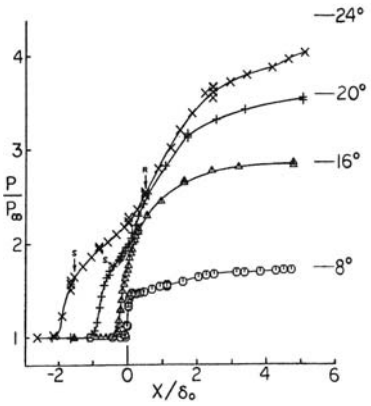

Figure 3: Surface-pressure distribution on various compression corner interactions at Mach 2.85 (Settles et al, 1978)

The influence of the compression on the turbulence is an enhanced mixing due to the formation of large-scale eddies (Kuntz et al., 1987) as the incoming boundary layer is driven out of equilibrium. The boundary layer mean flow recovery distance increases with increasing interaction strength (Smits and Muck, 1987; Selig et al., 1989; Ardonceau, 1984; Kuntz et al., 1987). The turbulence levels are strongly amplified across the shock system, and Selig et al. (1989) found that at Mach 2.9 the mass-flux fluctuations increased by more than a factor of four with a 24° turning angle. The flow distortion is also seen in the heat transfer. Evans & Smits (1996) found that the Reynolds analogy

	Re_θ	θ (mm)	δ^* (mm)	Cf	δ (mm)
Experiment	2400	0.43	2.36	0.00225	6.7
DNS	2100	0.38	1.81	0.00210	6.5

Table 1: Conditions for the incoming turbulent boundary layer at Mach 3.

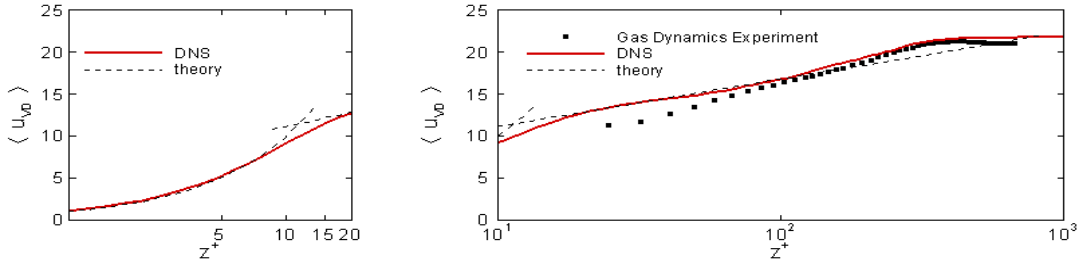

Figure 4: Comparison between the measured velocity profile and the DNS profile at Re_θ=2100 for the undisturbed boundary layer.

factor increased by a factor of three through a 16° interaction, and showed little sign of relaxation downstream of the corner.

DNS of a STBLI over a compression corner at Mach 3 and Re = 2100

In this section, we first consider the characteristics of the undisturbed boundary layer and we then study how the turbulence flow features are modified through the STBLI and how they recover downstream.

A. Undisturbed boundary layer

Table 1 lists the parameters for the incoming boundary layer given by the experiments and the DNS data. Figure 4 plots the van-Driest transformed velocity profile for the incoming boundary layer for the DNS, experiments and accepted inner and logarithmic layer correlations, showing good agreement. Figure 5 plots filtered Rayleigh scattering (FRS) images for the experimental data and density contours from the DNS. The resemblance between the experimental and DNS data is apparent. Experimentalists measure the turbulence structure angles using two probes separated by a distance ξ_y in the wall-normal direction. Then, the angle is defined by $\theta=\tan^{-1}(\xi_y / U_c\ \tau_{max})$, where U_c is the convection velocity (assumed to be equal to the local mean velocity) and τ_{max} is the time delay to the maximum in the space-time correlation for the mass flux (Alving & Smits, 1990; Alving et al., 1990). In the DNS data, we have the full three dimensional flow field, therefore we vary the streamwise location of the top probe and compute the spatial autocorrelation coefficient of mass flux to obtain the characteristic length scale ($U_c\ \tau_{max}$) as the streamwise distance from the bottom probe to the location where the autocorrelation peaks. Figure 6 plots the structure angles, the experimental data of Spina et al at Re = 80,000 are also plotted. The DNS data agrees well with the high Reynolds number data near the wall, for the same comparison the data do not agree near the boundary layer edge as the Reynolds number difference becomes apparent. Again, there is good agreement with the Bookey et al data.

Experiments in incompressible flow show evidence that hairpin-like structures cluster in streamwise-aligned groups known as 'packets' (Adrian *et al.*, 2000). The hairpin packet model explains the presence of extended, low-speed streaks in the buffer layer and fundamental aspects of the bursting event, and it is therefore a very important dynamical feature of turbulent boundary layers. Experiments indicate that the number of hairpins per packet increases with Reynolds number with a variation of three to ten per packet. The packet lengths range from 0.8-2δ, and the hairpin heads align to form 'ramps' with downstream angle of 12-20º. A hairpin packet is typically associated with a zone of low streamwise velocity below it, and packets are often nested. Ringuette et al. (2005) use these criteria and successfully identified hairpin packets in DNS data of turbulent hypersonic boundary layers.

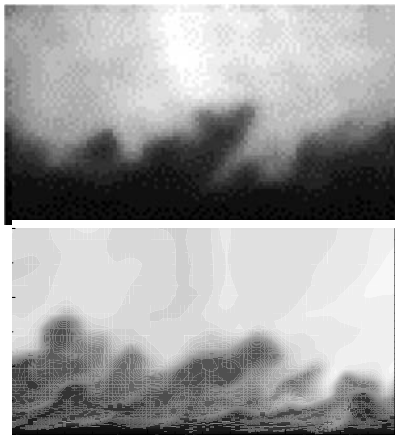

Figure 5: Filtered Rayleigh scattering from experiments (Top) and density contours from DNS (Bottom) for the undisturbed boundary layer. Flow is from left to right.

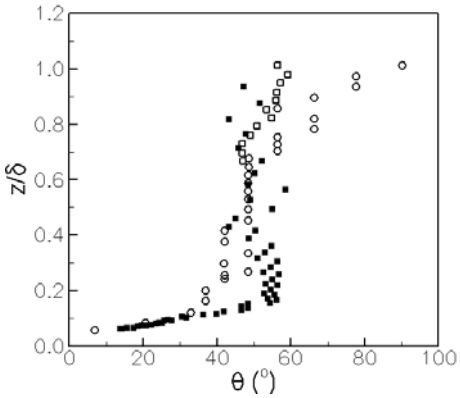

Figure 6: Turbulence structure angle for the undisturbed boundary layer from DNS and experiments. Solid symbols: DNS; circles: Spina et al; Empty squares: Bookey et al.

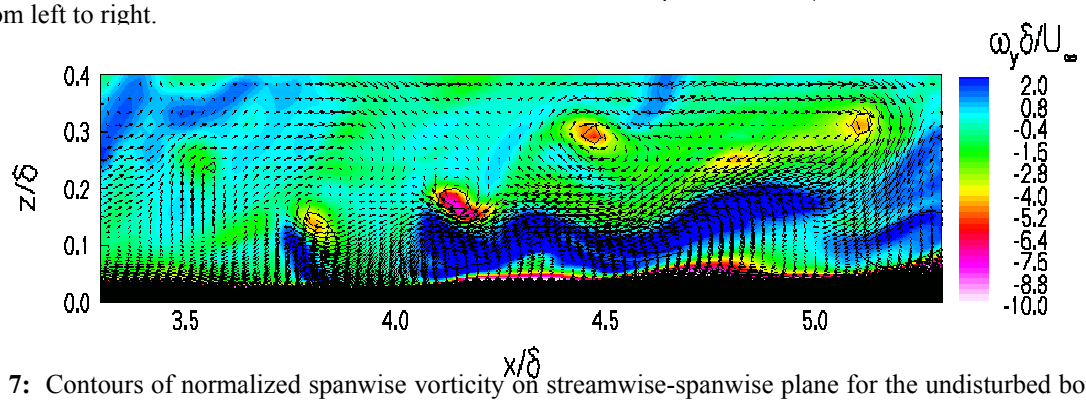

Figure 7: Contours of normalized spanwise vorticity on streamwise-spanwise plane for the undisturbed boundary layer form DNS. Relative velocity vectors are also superimposed, where $0.75U_\infty$ has been subtracted from the streamwise component.

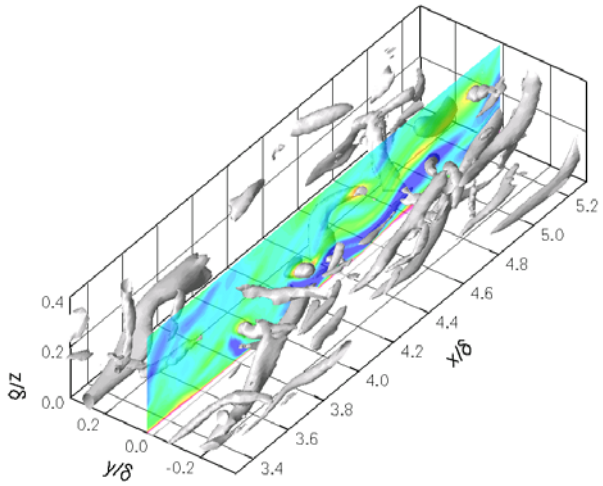

Figure 8: Iso-surface of swirl strength and contours of spanwise vorticity visualizing a hairpin packet in the undisturbed boundary layer from DNS data.

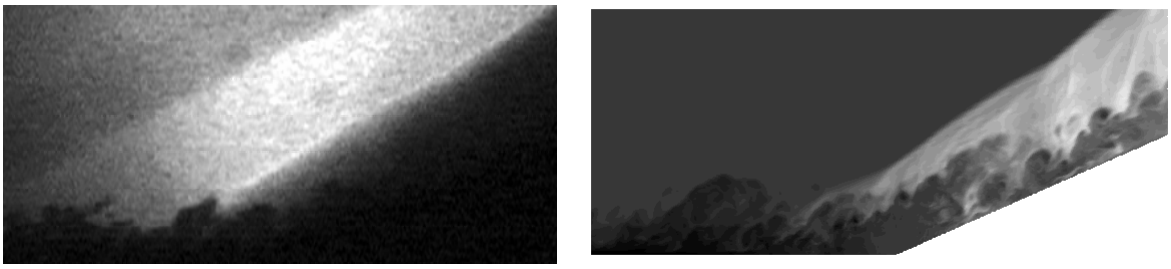

Figure 9: Filtered Rayleigh scattering from experiments (Left) and density contours from DNS (Right) for the STBLI. Flow is from left to right.

Using the procedure of Christensen & Adrian (2001), they first plot contours of spanwise vorticity on streamwise-wall-normal planes with velocity vectors superimposed, in a reference frame moving at 75% of the freestream velocity. In this way, they search for local regions of maximum vorticity, which might represent hairpin heads, and the alignment of such features at the corresponding angles of 12-20^o , which might represent hairpin packets. Then, iso-surfaces of swirl strength (Zhou et al., 1999), λci, are used to verify that such features are the signatures of three-dimensional coherent structures corresponding to packets. These results are illustrated in Figure 7, which plots contours of spanwise vorticity on streamwise-wall-normal planes with the velocity vectors superimposed on a Mach 3 turbulent boundary layer from DNS. The black lines are a single contour of swirl strength surrounding hairpin heads in regions of maximum vorticity with circular relative motion. Figure 8 plots contours of vorticity in the same plane and an iso-surface of swirl strength to visualize the three-dimensional hairpin packet. In the next section, we use the same analysis to track hairpin packets through the STBLI.

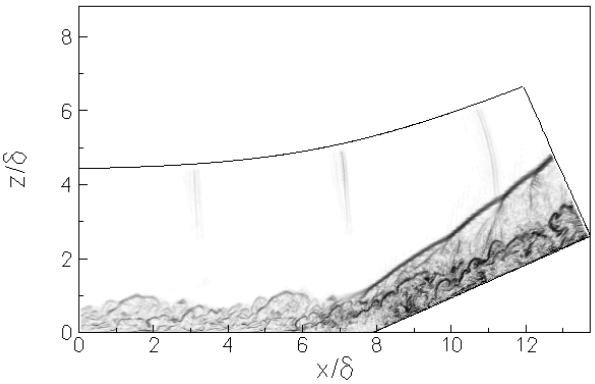

Figure 10: Numerical Schlieren for the STBLI from DNS

B. Compression Corner

Figure 9 plots FRS images and density contours for the experimental and DNS data for the 24^o compression corner at Mach 2.9 and Re_θ=2100. The shock angle and the turbulence structure appear similar in both cases. Figure 10 plots a numerical schlieren from the DNS data, showing the complexity of the flow downstream of the corner. The distortion of the turbulence through the interaction and the curvature of the main shock are apparent. Figure 11 plots the structure angle profiles at different streamwise locations. The compression corner is located at x=8δ, see Figure 10 for reference. Two locations, upstream and downstream of the corner within the interaction region are plotted. The structure angle clearly increases for z<0.4δ. For higher wall-normal locations, the structure angle appears to decrease slightly, although there is substantial scatter in the data. The turbulence structures are larger near the boundary layer edge and we believe that the angle data are not statistically converged in this region. The near-wall data suggest that in contrast to high Reynolds number flows, the structures are lifted up through the compression, indicating a substantial region of subsonic flow. Figure 12 plots contours of Mach number. The sonic line is near z/δ=0.4 and 0.7 for x=7.4δ and 9.4δ, respectively.

Figure 13 plots the streamwise integral length scale for various streamwise locations, see Fig. 10 for reference. Given the inhomogeneous character of the flow, the length scale is computed from the autocorrelation coefficient of fluctuating mass flux over volumes that span 1δ along the streamwise direction. In this way, the actual length scale

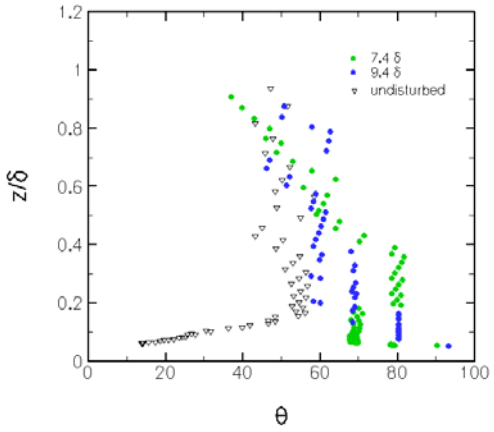

Figure 11: Structure angle profiles for two locations within the STBLI upstream and down stream of the corner from DNS.

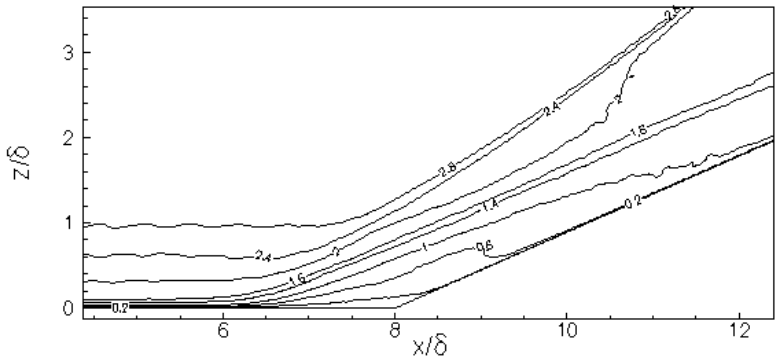

Figure 12: Contours of Mach number for the STBLI from DNS.

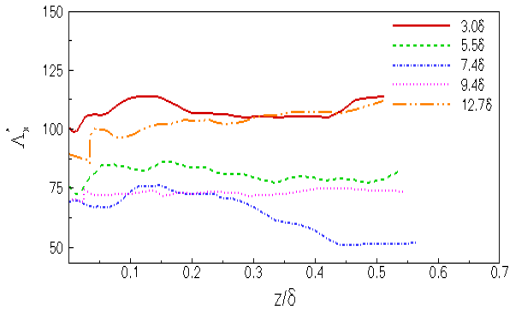

Figure 13: Normalized streamwise length scale profiles for different locations along the STBLI from DNS data.

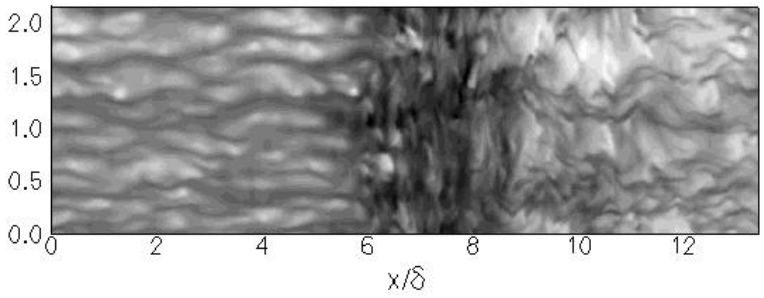

Figure 14: Contours of velocity on a streamwise-spanwise plane through the STBLI from DNS (Wu & Martin, 2004).

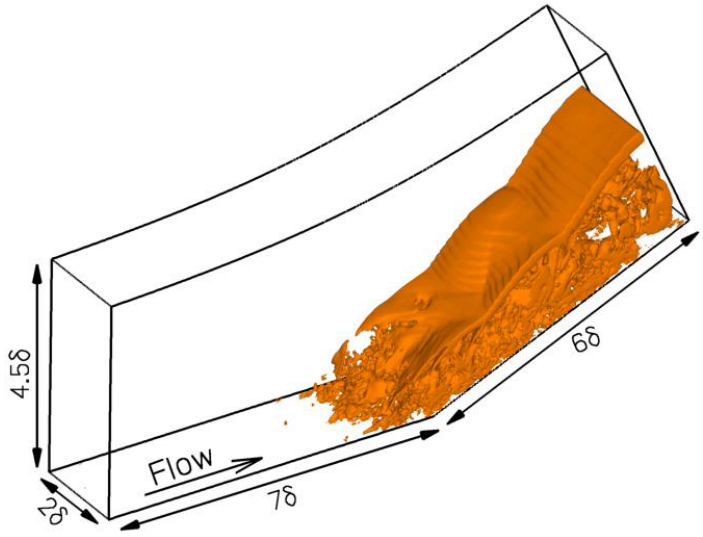

Figure 15: Iso-surface of $|\Delta P=3 \times 10^8$ (N/m^3) for the STBLI from DNS (Wu & Martin, 2004).

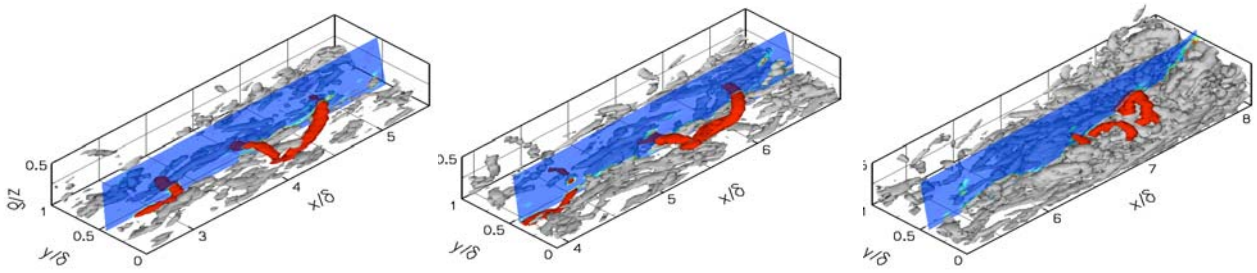

Figure 16: Iso-surface of swirl strength and contours of spanwise vorticity visualizing a hairpin packet through the STBLI from DNS data upstream of the corner. The hairpins within the packet are identified in red.

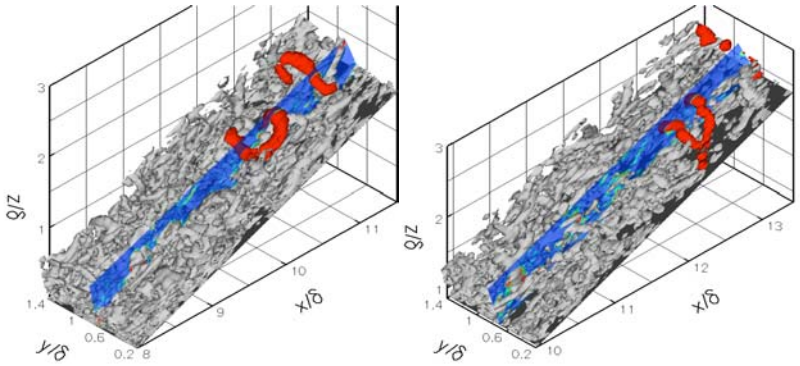

Figure 17: Iso-surface of swirl strength and contours of spanwise vorticity visualizing a hairpin packet through the STBLI from DNS data downstream of the corner. The hairpins within the packet are identified in red.

is not representative but rather the trend of its variation through the interaction is meaningful. The streamwise extend of the structures decreases through the interaction, upstream of the corner, and increases again downstream as the boundary layer recovers to equilibrium. Figure 14 plots contours of streamwise velocity at z+=5. The streaks can be observed for the undisturbed boundary layer. The coherence of these structures is lost through the interaction, and two large structures with a spanwise length of about δ form instead. These may be the signatures of Görtler vortices, which result from the concave curvature streamline pattern of the flow over the corner (Wu & Martin 2004). Figure 15 plots an iso-surface of the magnitude of the pressure gradient, also showing the three-dimensionality of the shock with the corresponding 2δ wavelengths. Figures 16 and 17 plot the convection of a hairpin packet through the interaction at locations x=3.0δ, 5.5δ, 7.4δ and 9.4δ, and 12.8δ. The coherence of the packet gets lost between 7.4δ and 9.4δ, and we are able to track another packet downstream of the corner as the boundary layer recovers.

Using the shock-search algorithm of Taylor and Martin (2005), we find the statistical strength of the shocks through the interaction. Figure 18 plots the probability density function of normal shock strength, M_n, for the STBLI. The data are post-processed in two separate regions, namely in 4δ –10δ and 11δ - 15δ. For both data sets, the PDFs exhibit two large peaks. The first peak represents the strength of the shocklets within the boundary layer, being about M_n=1.1. The second large peak represents the strength of the main shock, being about M_n=1.5 for the upstream data and 1.9 for the downstream data. High Reynolds number experiments show that the main shock strength is weaker than that of the inviscid flow near the corner, and it matches the inviscid strength downstream of

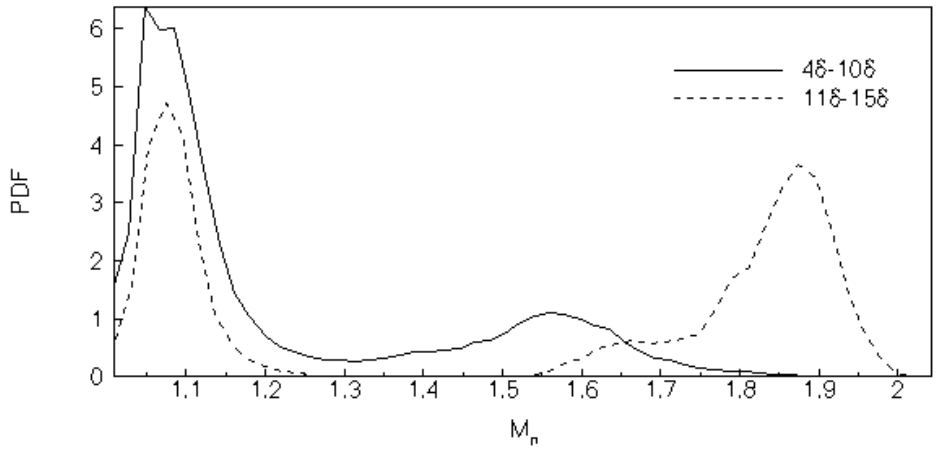

Figure 18: Probability density function of shock strength, which is given relative to the normal shock Mach number, for the STBLI from DNS data.

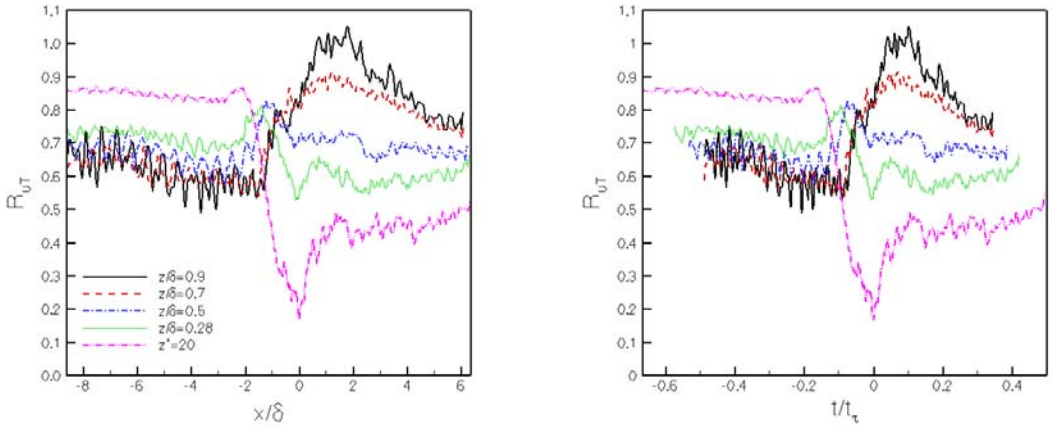

Figure 19: Reynolds analogy factor through the interaction along the streamwise direction (Left) and in a time reference non-dimensionalized by the incoming boundary layer properties $\tau=\delta/u_\tau$ (Right). The x-coordinate axes have been normalized so that they are centered at the compression corner.

the interaction. The downstream data also exhibits a third peak, representing the two-shock system present in this data set, that is one weaker shock and one of inviscid strength appear consecutively along the streamwise direction.

Figure 19 plots the negative correlation coefficient of velocity and temperature fluctuations or Reynolds analogy factor, R_{uT}, through the interaction at various wall-normal locations. The data are plotted along the streamwise direction and in a time frame using $t=x/U_c$ and $\tau=\delta/u_\tau$ for the undisturbed boundary layer as the normalization time unit. For the subsonic portions of the boundary layer downstream of the corner, R_{uT} appears to converge quickly to values between 0.4 and 0.6. For the supersonic portion of the boundary layer, however, R_{uT} increases slowly through the interaction and then slowly decays in a trend to recover to the original equilibrium value. DNS studies of compressible turbulent boundary layers (Martin, 2005) show that a disturbed boundary layer takes about 1.5 to $2\delta/u_\tau$ units to recover to equilibrium. Based on the results from Fig. 18, the boundary layer may be expected to recover to equilibrium nearly 22 to 30 boundary layer thicknesses downstream of the interaction.

Conclusions

Direct numerical simulations provide a vast amount of accurate and detailed data that can be used to develop a greater understanding of fundamental physical phenomena and to develop and validate turbulence models that are true. In this paper we have presented a brief summary of the STBLI over a compression corner configuration from previous experimental data. Additional details of this flow are presented from the DNS data of a Mach 3 and Re_θ = 2100 configuration. The post-processing procedures to analyze the DNS data are first presented in the undisturbed boundary layer and are then used to analyze the disturbed flow through the interaction. The turbulence enhancement downstream of the interaction is apparent from numerical schlieren images. We find that for the lower Reynolds number data, the boundary layer downstream of the interaction has a significantly large subsonic region, extending up to nearly 0.7δ. In turn, the compression results in increased angles of the turbulence structure within the subsonic regions. The statistical data suggest a trend of decreasing angle in the supersonic region; however, the data are not converged. The increase in angle for these regions can be observed in the instantaneous density contour plots and schlieren images. Hairpin packets are identified and followed through the interaction. These coherent structure packets are lost near the compression corner. The statistics show the presence of shocklets with normal Mach number strength of 1.1 within the boundary layer upstream and downstream of the interaction. In addition, the data also describe the presence of a two-shock system with a weaker shock and a shock of inviscid strength appearing consecutively along the streamwise direction. The Reynolds analogy factor indicates the trend of recovery to equilibrium for the boundary layer downstream of the interaction. In the subsonic regions of the boundary layer, the factor is below 0.8. The recovery of the factor to equilibrium is much slower in the supersonic regions. According to recent DNS studies of compressible turbulent boundary layers (Martin, 2005), the boundary layer is expected to recover to equilibrium nearly 22 to 30 boundary layer thicknesses downstream of the interaction.

Acknowledgements

This work is supported by the Air Force Office of Scientific Research under grant AF/F49620-02-1-0361.

References

1. Adams, N.A., "Direct simulation of the turbulent boundary layer along a compression ramp at M=3 and Reθ=1685,'' Journal of Fluid Mechanics, 420, 4 (2000).

2. Adrian, R.J., Meinhart, C.D., Tomkins, C.D., "Vortex Organization in the outer region of the turbulent boundary layer," 422, pp. 1-54, 2000.

3. Alving, A.E, and Smits, A.J., "Correlation measurements and structure angles in a turbulent boundary layer recovering from convex curvature," in: Kline, S.J. & Afgan, N.H. (eds), Near-Wall Turbulence. Hemisphere.

4. Alving, A.E., Smits, A.J., and Watmuff, J.H., "Turbulent boundary layer relaxation from convex curvature," Journal of Fluid Mechanics, 211, 529-556.

5. Ardonceau, P.L.,"The Structure of Turbulence in a Supersonic Shockwave/Boundary Layer Interaction," AIAA Journal 22, 9 1254-1262, 1984.

6. Bookey, P., Martin, M.P., and Smits, A.J., "New Experimental Data of STBLI at DNS/LES Accessible Reynolds Numbers," AIAA Paper No. 2005-0309, 43rd Aerospace Science Meeting and Exhibit, Reno, NV, January 2005.

7. Christensen, K.T., and Adrian, R.J., "Statistical Evidence of Hairpin Vortex Packets in Wall Turbulence," Journal of Fluid Mechanics, 431, pp. 433-443, 2001.

8. Dolling, D. and Murphy, M., "Unsteadiness of the Separation Shockwave in a Supersonic Compression Ramp Flowfield," AIAA Journal 21, 12, 1983.

9. Erengil, M.E., and Dolling, D.S., "Unsteady Wave Structure near Separation in a Mach 5 Compression Ramp Interaction," AIAA Journal, Vol. 29, No. 5, pp. 728-735, 1991.

10. Evans, T., and Smits, A.J., "Measurements of the Mean Heat Transfer in a Shock Wave Turbulent Boundary Layer Interaction," Experimental Thermal and Fluid Science, 12, 87-97 (1996).

11. Knight, D., Tan, H., Panaras, A., and Zheltovodov, A. "RTO WG 10: CFD Validation for Shockwave Turbulent Boundary Layer Interactions," AIAA Paper No. 2002-0437, 2002.

12. Knight, D., "RTO WG 10: Test Cases for CFD Validation of Hypersonic Flight," AIAA Paper No. 2002-0433, 2002.

13. Kuntz, D.W., Amatucci, V.A., and Addy, A.L., "Turbulent Boundary Layer Properties Downstream of the Shockwave/Boundary-Layer Interaction," AIAA Journal 25, 5, 668-675, 1987.

14. Martin, M.P., "DNS of Hypersonic Turbulent Boundary Layers. Part I: Initialization and Comparison with Experiments," Submitted to Journal of Fluid Mechanics, 2005.

15. Martin, M.P., Taylor, E.M., Wu, M., and Weirs, V.G., "A Bandwidth-Optimized WENO Scheme in Direct Numerical Simulations of Compressible Turbulence," Submitted to Journal of Computational Physics, 2005.

16. Ringuette, M., Martin, M.P., and Smits, A.J., "The Structure of Supersonic Turbulent Boundary Layers from DNS Data," APS DFD Meeting, Chicago, IL, Nov. 20-22, 2005.

17. Rizzetta, D.P. & Visbal, M.R., "Large-Eddy Simulation of Supersonic Compression Ramp Flow by High-Order Method," AIAA Journal 39, 2283-2292, 2001.

18. Selig, M.S., Muck, K., Dussauge, J., and Smits, A.J. , "Turbulent Structure in a shock Wave/Turbulent Boundary Layer Interaction," AIAA Journal, 27, 7 862-869, 1989.

19. Settles, G.S., Bogdonoff, S.M., and Vas, I.E., "Incipient Separation of a Supersonic Turbulent Boundary Layer at High Reynolds Number," *AIAA Journal* 14, 1 50-56, 1976.

20. Settles, G.S., Fitzpatrick, T.J., and Bogdonoff, S.M., "A Detailed Study of Attached and Separated Compression Corner Flowfields in High Reynolds Number Supersonic Flow," AIAA Paper No. 1978-1167, 1978.

21. Settles, G., Vas, I., and Bogdonoff, D., "Detailed Study of Attached and Separated Compression Corner Flowfields in High Reynolds Number Supersonic Flow," AIAA Journal 17, 6, 1979.

22. Sinha, K. & Candler, G.V. (2005) "Shock and Turbulent Boundary Layer Interaction in Hypersonic Flows," Workshop on STBLI, 43rd AIAA Aerospace Sciences Meeting and Exhibit, January.

23. Smits, A.J., and Muck, K.,"Experimental Study of Three Shockwave/Turbulent Boundary Layer Interactions," Journal of Fluid Mechanics, 182, 291-314, 1987.

24. Taylor, E.M., and Martin, M.P., "Local Stencil Adaption Properties of a WENO Scheme in Direct Numerical Simulations of Compressible Flows," Submitted to Journal of Scientific Computing, 2005.

25. Taylor, E.M., Wu, M., and Martin, M.P., "Optimization of Nonlinear Error Sources for Weighted Essentially Non-oscillatory Methods in Direct Numerical Simulations of Compressible Turbulence," AIAA Paper No. 2006-1091, 44th Aerospace Science Meeting and Exhibit, Reno, NV, January 2006.

26. Verma, S.B. "Experimental study of flow unsteadiness in a Mach 9 compression ramp interaction using a laser schlieren system," *Meas.Sci.Technol.* 14, pp. 989–997, 2003.

27. Wu, M. and Martin, M.P., "Direct numerical simulation of shockwave/turbulent boundary layer interaction," AIAA Paper No. 2004-2145, 34th AIAA Fluid Dynamics Conference, Portland, Oregon, June 2004.

28. Wu, M., E.M. Taylor, and Martin, M. P, "Assessment of STBLI DNS Data and Comparison against Experiments," AIAA Paper No. 2005-4895, 35th AIAA Aerospace Science Meeting and Exhibit, January 2005.

29. Wu, M., and Martin, M.P., "Assessment of Numerical Methods for DNS of Shockwave/Turbulent Boundary Layer Interaction," AIAA Paper No. 2006-0717, 44th Aerospace Science Meeting and Exhibit, Reno, NV, January 2006.

30. Zheltovodov, A.A. (2004) "Advances and Problems in Modeling of Shockwave Turbulent Boundary Layer Interactions," Proceedings of the International Conference on the Methods of Aerophysical Research, Novosibirsk, Russia, Part I, 149-157.

31. Zhou, J., Adrian, R.J., Balachandar, S., and Kendall, T.M., "Mechanisms for generating Coherent Packets of Hairpin Vortices in Channel Flow," Journal of Fluid Mechanics, 387, pp. 353-396, 1999.